nature physics

SUPPLEMENTARY INFORMATION

DOI: 10.1038/NPHYS2257

The organization of strong links in complex networks

Sinisa Pajevic[1] and Dietmar Plenz[2]

[1]*Mathematical and Statistical Computing Laboratory, DCB/CIT, NIH*

[2]*Section on Critical Brain Dynamics, LSN, NIMH*

1. Topological measures of clustering in networks

Node clustering coefficient.

For each node *i*, the node clustering coefficient, C_i, was defined as the probability that an edge between any two of its neighbours exists [1]. This concept is easily extended for directed networks, i.e.,

$$C_i = \frac{\sum_{j,k\in\Omega_i} a_{jk}}{k_i(k_i-1)}, \qquad \text{(S1)}$$

where Ω_i contains all neighbours of node i and a_{jk} is an element of the adjacency matrix so that $a_{jk} = 1$ if a directed link from j to k exists, otherwise it is zero. The clustering coefficient C of a network is the average of C_i for all nodes with degree 2 or greater. For directed networks, Ω_i and, hence, C_i can be defined based on the '*out*', '*in*', or '*all*' neighbourhood utilizing either the out-going, in-coming, or all of the links of a node respectively. If not stated otherwise, our analysis for directed networks is based on '*out*'-neighborhood.

Link Clustering Coefficient

For any directed or undirected link, we define the neighbourhoods for each of its end nodes, either by choosing nodes that it points to (*out* neighbourhood), nodes that point to it (*in* neighbourhood) or without considering direction (*all* neighbourhood), noting that a different type of the neighbourhood can be chosen for the source and the target node. Then, the whole set of pure neighbours (that exclude the source and the target nodes themselves) can be divided into three groups: the common nodes, n_C , and two sets that are unique to the source and to the target. In clustered networks the number of common nodes will be much larger than in the equivalent randomized network, and hence we use it as a local measure of clustering defined for each link. More precisely, the link clustering coefficient, C_L, for a given link is defined as

$$C_L = \frac{n_C}{n_T}, \tag{S2}$$

Where n_C is the number of common neighbours of the link's end nodes, and n_T is the total number of end node neighbours excluding the end nodes themselves (see Figure 1a main). We developed two quantitative measures to study the relationship of link weight w and C_L in weighted networks.

A similar measure of clustering local to the edges, called *edge clustering*, has been defined in ref [2] as the fraction of the triangles passing through an edge out of the total possible number of triangles that could potentially exist between the neighbours. This can be written as

$$C_{i,j}^{(3)} = \frac{z_{i,j}^3}{\min[(k_i - 1),(k_j - 1)]},$$

where $C_{i,j}^{(3)}$ is the edge coefficient, $z_{i,j}^{3}$ is the number of triangles passing through the edge (i,j), and k_i and k_j are the degrees of the end nodes of the edge. For undirected networks this measure differs from C_L only in the way it is normalized. However, our measure is a more conservative measure of clustering and our definition enables easier adoption to directed networks by merely changing the definition of neighbourhood. Thus, by taking into consideration the direction of the link between the two end nodes as well as their neighbours, we have examined 5 of the total 9 pairs of neighbourhood schemes (out-out, in-in, all-all, in-out, out-in; see Suppl. Fig. S6a). We have also explored many different normalization schemes, including the one used for edge clustering coefficient, none of which changes the nature of correlations with weights significantly.

Excess Clustering

In our analysis, we use *excess clustering*, ΔC, which we define as the difference between the clustering coefficient of the original network, C^{orig}, and that of an equivalent randomized network, C^{DSPR}, with the degree sequence preserved (DSPR [3]),

$$\Delta C = C^{orig} - C^{DSPR}, \tag{S3}$$

The reason for preferring ΔC over C is that C can indicate high clustering even when it arises trivially from the prescribed node degree sequence or degree distribution. Notably, any complete graph has $C = 1$. On the other hand, for a network to have significant ΔC, some form of targeted connectivity ought to be present in network formation. It is widely accepted that true clustering requires the presence of diverse node groups and some

preference of attaching to one group over the others are required [4-7], which in general can arise through the presence of hidden metric spaces[8, 9].

Technically, we obtained DSPR networks by repeated random selections of a pair of directed links with distinct source and target nodes, and then switching the target nodes. The number of switches was twice the total number of links. At each pruning level, we estimated ΔC by averaging over a certain number of randomized networks (with slightly different values of C^{DSPR}), which ranged from 2 randomizations for networks larger than 10,000 nodes and up to 20 for the smallest networks..

WN and OHO network topologies

In our models, we tested two common small-world topologies. The Watts-Newman topology (WN)[10] is a simpler version of the Watts-Strogatz topology[1]. Long range random links are added to a regular lattice connecting K nearest neighbors without rewiring the existing lattice links. In essence, it is a simple superposition of an Erdos-Renyi network with a regular lattice network. In our implementation, we use K = 4 and p = 2/N, yielding average degree of 10. The Ozik-Hunt-Ott (OHO)[11] topology is a growing network model which starts with a simple lattice to which new nodes are inserted in between two randomly chosen neighbors and forming links to K nearest neighbors. This model yields a highly clustered network with C ~ 0.7 which is independent of N and exponentially distributed degree distribution. We used K = 6, for which the average degree is 12.

2. Supplementary Analysis

Alternative measure of correlation between weights and clustering

We showed that an integrative weight organization can be introduced in typical small-world topologies by assigning link weights w_{ij} proportional to the clustering coefficients of the corresponding end nodes *i* and *j* as in Eq. 3 in the main text. This assignment results in high positive values for *M* and R_{C_L}. In addition, we studied the correlation R_w between the weights in the original network, *w,* and those assigned by the Eq. 3 in the text, i.e.

$$R_w = \mathrm{Corr}(w_{ij},\, C_i \cdot C_j)\,. \qquad \text{(S4)}$$

We calculated R_w for natural and simulated networks and found, as shown in Suppl. Fig. S9 that R_w correlates with R_{C_L} (R = 0.73).

Relationship between R_{C_L} and M

Many global network characteristics can be explained in terms of local interaction rules, e.g. a scale free degree distributions can arise from a local preferential attachment rule Barabasi [12]. In the current study, our results imply that the observed invariance of clustering and its global robustness to the loss of weak links, as measured with *M* is related to the local weight-clustering correlations in integrative networks, quantified with R_{C_L}. If the relationship is deterministic then tuning the value of R_{C_L} would provide the means for a network to achieve desired global properties, e.g. high modularity[13] or in our case the robustness of clustering in which the average clustering coefficient is nearly

invariant to the loss of weak links. While we observe high correlation between R_{C_L} and M in real world networks, we see that within each quadrant the correlation between the two is not strong. It appears intuitive that having higher weights in clustered neighbourhoods will be more likely to preserve its clustered nature when the weak links are removed, however achieving the invariance in *C* is not guaranteed by the presence of positive R_{C_L}. The precise relationship between the two variables is difficult to determine, and certainly it would be unwarranted to suggest that the local integrative nature causes or determines the robustness. Since in any particular real world network we cannot vary R_{C_L}, we turn to models in order to determine what effect it has on robustness. In many weighting models that can reproduce the local integrative property, i.e. high R_{C_L}, we find that *M* is not necessarily very high. We also find that variations in R_{C_L} are often uncorrelated or negatively correlated with variations in *M*. For example, in figure S8a we plot *M* vs. R_{C_L} during 'learning at last step' (data taken from Fig. 6 main text). The tortuous trajectory of this recurrence plot reveals the complex relationship between the two variables during learning. In fact, after a brief initial period, *M* and R_{C_L} are negatively correlated (R=-0.24) . Similarly, in a recent social network model [13], when varying the main parameter (see the section on Growing Networks), integrative networks with varying R_{C_L} are produced, however *M* tends to be in the lower half of the first quadrant and the two variables are only weakly correlated (see Fig. S8b, correlations reported in the figure).

Thus it appears that R_{C_L} provides some constraints on the domain of *M* values, however, its precise boundaries are difficult to obtain. A constraint between *M* and R_{C_L} that can be

precisely established is that for independent weights both are expected to be zero, i.e. fixed to the origin (see Appendix, main text). It also appears from many examples studied here, and intuitively, that positive R_{C_L} leads to positive *M* and vice versa, thus, they tend to appear in the first and third quadrants of *M* vs. R_{C_L} plots. On the other hand, we already know that some of the real world networks examined in our study violate these constraints. For example, the *C. elegans* network yields high M, but negligible R_{C_L} and the US airports network shows positive R_{C_L}, but slightly negative *M*. In order to test these constraints further, we introduce a weighting scheme that creates a tension between high *M* and R_{C_L}. It utilizes the fact that the weighting model in Eq.3 (main text) produces high *M*, but not as high R_{C_L} as one would obtain if C_L was used directly to develop a weighting scheme. We balance the two opposing weighting tendencies with a parameter, *a*. More specifically, we applied weights according to

$$w_{ij} \sim C_i \cdot C_j - aC_L^{(i,j)}, \qquad \text{(S5)}$$

where *a* is a control parameter which we studied for a wide range of values ranging from much smaller than 1 (0.01) to much larger than 1 (100) spaced logarithmically. We identify a range of *a* for which the measures had different signs, i.e. fall outside the Upper-Right and Lower-Left quadrants of Fig. 4. Indeed, as shown in Fig. S8c, in which the weighting scheme was applied for OHO and WN topologies, the measure can take on opposite signs. We also note that for a wide range of negative values of R_{C_L}, the two measures were either uncorrelated (OHO; Fig. S8c, top) or even slightly anti-correlated

(WN; Fig. S8c, bottom), and that for WN topology the trajectory does not pass through the origin (Fig. S8c, arrow) .

Giant Component and Mean Path Length Pruning Analysis

Results of pruning will also depend on the initial level of sparsity in the network and the network pre-processing. For example, for a fully connected, i.e. complete network, the excess clustering is zero and hence an increase in ΔC is to be expected. For the fMRI functional network, we established an independent and commonly used threshold, thus declaring the default level of significance in measured correlations. In gene and actor networks, due to their extremely large size we were forced to omit the weakest links. Since the pruned networks exhibited robustness to bottom pruning, we could proceed consistently. We note that care has to be taken that such pre-processing does not change the character of the network.

3. Description of networks analyzed

Sources of weighted networks

The weighted networks used in the present study were obtained from numerous sources. Neuronal avalanche networks were obtained from our own laboratory, DSI and fMRI networks were obtained from the group of Olaf Sporns, but the majority of the networks were obtain from the following three sources/databases: 1) the data provided by Mark EJ Newman at http://www-personal.umich.edu/~mejn/netdata/ , 2) Pajek (a software program for large network analysis) website, originally found at http://vlado.fmf.uni-lj.si/pub/networks/pajek/ but has since migrated to http://pajek.imfm.si/doku.php , 3)

University of Florida Sparse Matrix Collection (UFSMC) at http://www.cise.ufl.edu/research/sparse/matrices/ which is also hosted at http://aws.amazon.com/datasets/Mathematics/2379. One can also search this database at http://www2.research.att.com/~yifanhu/GALLERY/GRAPHS/search.html or at http://aws.amazon.com/datasets/Mathematics/2379. We now provide more details about each of the networks (network groups) studied.

Weighted neuronal avalanche networks (Avalanche networks, n = 3)

Functional cortical architectures of neuronal avalanches represent weighted directed networks derived as described previously [14]. In short, spontaneous synchronized activity was recorded in organotypic cortex slices cultured on integrated, planar 8x8 multi-electrode arrays (MEA) [15]. The local voltage fluctuations at each electrode site was thresholded and the time series of suprathreshold events at each electrode was taken as node activations in a 60-node networks (corner electrodes were not present). Cascades of node activations have been shown to form spatiotemporal clusters whose size distributions obey a power law with slope of -1.5, the hallmark of neuronal avalanches. By observing the spatio-temporal evolution of node activities on the network, a directed, weighted graph is derived [14]. The first data set was based on 7 cultures with stationary avalanche rate [15]. In a second data set, avalanche rate changed by an order of magnitude due to external slow driving [16]. We used three data sets to study functional neuronal avalanche connectivity in awake macaque monkeys. The first data set was derived from monkey 1 described in [17] based on ongoing avalanche activity in premotor cortex (N = 32 microelectrodes). The 2nd and 3rd data sets were obtained in 2 other awake, quietly sitting

macaque monkeys (NIMH) by recording ongoing avalanche activity in the premotor cortex with 10x10-electrode arrays (0.6 mm interelectrode distance; N ~ 100). Functional architectures were reconstructed as described in [14] using a time step of 2 ms and an LFP threshold of -2.5 SD of signal fluctuations.

Structural and functional human cortex core (Human Brain, n = 2)

The structural and functional connectivity data of the human cerebral cortex from the same 5 human subjects was recently published [18] and is available at http://www.indiana.edu/~cortex/resources.html. The nodes in these networks represent cortical regions of interests (N = 998) distributed over 66 functional cortical areas. The structural human cortex core has been identified using diffusion spectrum imaging (DSI) which includes ~15,000 fiber bundles of various densities that reflect the connection capacity between regions. The functional connectivity was based on correlations in the resting BOLD signal of fMRI between the same N = 998 cortical regions of interest. Since such a network is fully connected (complete), we obtained the sparse functional networks by keeping only those links for which pair-wise correlations *R* in the fMRI signal were larger than 0.2.

Gene regulatory networks (Gene, n = 3)

We used two human gene regulatory networks (N≅ 22300 and 14300) and one mouse network (N≅45100). They were obtained from the University of Florida Sparse Matrix Collection (UFSMC), posted by Vicenzo Belcastro's group, and described in [19]. Nodes in these networks represent individual genes and the links between them relate the

expression level of each gene with the expression of other genes. The weights do not represent correlations, but rather a value of a parameter value in ODE-based algorithm, NIR [20]. Due to the large size of these networks and a very large number of significant links, we studied networks that were either sub-sampled versions of the original networks (see Suppl Figure 1 for networks sub-sampled at N = 1000 and N = 2000 nodes) or in which only links with an interaction parameter greater than 0.08 were kept, yielding very sparse networks that could be analyzed in a reasonable amount of time. Either method led to the same conclusion in terms of our pruning and link clustering analysis. The sub-sampled versions produced very similar results and were robust even if only 1000 or 2000 nodes were used in sub-sampling (see Suppl. Fig. S1). The results were also similar to those of the thresholded networks with the full set of nodes shown in Fig. 1e.

Actor Collaboration Network (Actor, n = 1)

The actor networks were reconstructed using data from the Internet Movie Database (IMDb), provided by the Pajek Group provided in a Matlab format on the Pajek website http://pajek.imfm.si/doku.php. The original data contained a bipartite graph connecting 428K movies to 896K actors that were participating in them. From this bipartite graph, we reconstructed a weighted network in which the nodes represent actors and the link weights represent the number of movies in which they appeared together. To make this network computationally manageable, we first only considered movies with more than 5 actors in it and for the following categories: Drama, Short Documentary, Comedy, Western, Family, Mystery, Thriller, Music, Crime, Sci-Fi, Horror, War, Fantasy, Romance, Adventure, Animation, Action, Musical, Film-Noir. Second, we only kept

actors who appeared in at least 10 movies. The final network had N = 53K nodes and its properties are listed in Table I.

"Les Miserables" Characters network (Les Miserables, n = 1)

The co-appearance network of characters in the novel *Les Miserables* has 77 nodes and weights represent the number of chapters in which a pair of characters appeared together. This network was originally created and studied in [21] and was obtained from the MEJ Newman web-site (http://www-personal.umich.edu/~mejn/netdata/).

Words co-occurrence and Free Association Networks (Words, n = 2)

We used two different word networks. In the word co-occurrence *Reuters News 9/11* network, nodes represent keywords that occurred together in *Reuters News* articles on September 11, 2001 , the day of the terrorist attacks in USA. The link weights represent the frequency of their co-occurrence. Originally produced by Steve Corman and Kevin Dooley at Arizona State University, the data are publicly available at http://pajek.imfm.si.

The *Free Association Word network* (FA Word) is a directed network, in which source nodes represent normed words/cues to which >6,000 participants were asked to write the first word, the target node, that came to mind that was meaningfully related or strongly associated to the presented word,. The mechanics of this survey consists of a long list of words with the blank shown next to each item. For example, if given BOOK _____, they might write READ on the blank next to it. This procedure is called a discrete association task because each participant is asked to produce only a single associate to each word. This network can be found on the *Pajek* (http://vlado.fmf.uni-lj.si/pub/networks/data/dic/fa/FreeAssoc.htm), or USF website (http://w3.usf.edu/FreeAssociation/AppendixA/index.html).

For additional details see also http://w3.usf.edu/FreeAssociation/Intro.html.

Caenorabditis elegans (*C. elegans*) Network

The neural system of the nematode worm *C. elegans* is comprised of a total of N = 302 neurons, most of which are linked together into one large, network. Our calculations are based on three versions of this network. We used a recently improved *C. elegans* neuronal data base [22] that contains one network based on chemical, i.e. synaptic, connections and one network based on electrical, i.e. gap-junction, mediated connections between neurons (available at http://mit.edu/lrv/www/elegans/). Link weights in these networks represent multiplicity of connections between neurons. For comparison, we also analysed an earlier version of this network [23] with its small-worldliness introduced in [1] and which is available at http://www-personal.umich.edu/~mejn/netdata/. Results for all three networks did not differ substantially and were averaged for presentation purposes.

Scientific author collaboration networks (Collaboration Networks, n = 4)

In author collaboration networks, authors from different disciplines in physics represent nodes and are connected, if they co-author a paper. Link weights in these networks quantify the number of papers co-authored, each paper carrying the weight inversely proportional to the total number of the authors. The disciplines 'Condensed Matter', 'Network Sciences', 'High Energy Physics', and 'Astrophysics' with N = 1,500 – 17,000 authors, i.e. nodes, were analysed (available at http://www-personal.umich.edu/~mejn/netdata/).

Airline transportation network (Transportation Networks, n = 2)

The US Air airline network is an undirected, weighted transportation network with N = 332 nodes representing airports around the world. Link weights represent the relative number of the flights US Air had in 1997 (http://www.cise.ufl.edu/research/sparse/matrices/Pajek/USAir97.html). We also used an airport network (http://wiki.gephi.org/index.php/Datasets) in which the nodes constitute 500 airports in the US and link weights represent the number of passengers transported each year.

Weighted Growing Networks

We created networks based on two popular models of weighted evolving networks, i.e., in which weights are assigned during growth as nodes and links are added. The two growth models (GM) assign weights according to (1) resources reserved based on the degree of the connecting node [24] or (2) fixed resources distributed based on the relative node strengths [25]. These two rules were originally applied to preferential attachment models and as such did not produce networks with any excess clustering. We therefore applied the corresponding weight assignment rules to the OHO [11] growing network, which has significant ΔC and named them (1) GM1 OHO and (2) GM2 OHO.

Social Network Weighting Model

In this weighting social network model[13] (SN) the weights and links evolve in time, while the number of nodes is kept fixed throughout. It uses local neighbourhood searches to increase the number of common neighbours and corresponding link weights.

The two critical model parameters that we varied are the relative weight increase for closed triangles, δ, which we studied for 3 different values (δ = 0.25, 0.5, and 1, and on a network with size N = 100 and 500), and p_Δ, a probability that a neighbour of a given nodes neighbour will form a new connection if the one did not exist (p_Δ =0.001 and 0.005). Except for the size of the networks being smaller, the other parameters being set are similar to the ones used in Kumpula et al. [13] Since we use smaller networks the average degrees in our networks were closer to 5, rather than 10 reported in [13], and we did not tune p_Δ to achieve the desired characteristics. For us this model was just the means to explore further the relationship between the local weight-clustering correlations and the robustness, hence the precise implementation of the networks with the same characteristics was of lesser importance.

4. Supplementary Table

Table 1: *Summary of network properties*. The first column contains the network name and the number of actual networks analyzed in parenthesis. The data columns are as follows: *N*: number of network nodes. <*k*>: mean node degree. <*d*>: mean network diameter. r_A : assortativity based on degree-degree correlations. *C*: average node clustering coefficient. *ΔC*: mean excess clustering. *Q*: Network modularity obtained using Girvan-Newman algorithm [26, 27]. *M* and R_{C_L} as defined in the main text.

Networks (#nets)	N	$\langle k \rangle$	$\langle d \rangle$	r_A	C	ΔC	Q	M	R_{C_L}
Neural									
DSI Human Brain (5)	998	36	3.1	0.29	0.47	0.42	0.68 ± 0.08	0.34	0.59
fMRI Human Brain (5)	998	67	2.7	0.25	0.53	0.44	0.62	0.56	0.63
Avalanche Monkey (3)	77 ± 14	13 ± 4	2.6 ± 0.19	0.3 ± 0.13	0.51 ± 0.03	0.29 ± 0.03	0.48 ± 0.03	0.39	0.45
Avalanche Culture (7)	59	16 ± 3	2.3 ± 0.17	0.28 ± 0.11	0.63 ± 0.03	0.32 ± 0.03	0.5 ± 0.06	0.65	0.31
Aval. Culture Driven (7)	58 ± 1	16 ± 4	2.2 ± 0.16	0.24 ± 0.11	0.57 ± 0.03	0.26 ± 0.03	0.41 ± 0.07	0.72	0.22
C-elegans (3)	285 ± 10	7.9	3.6 ± 0.3	0.02 ± 0.07	0.23 ± 0.01	0.15 ± 0.01	0.5 ± 0.04	0.4	0.002
Transportation									
US Air (1)	332	13	2.7	-0.21	0.75	0.24	0.2	-0.19	-0.025
US airports (1)	500	12	3	-0.27	0.73	0.18	0.28	-0.059	0.31
Human									
Actors (1)	53960	6.6	7.6	0.18	0.58	0.53	0.68	0.47	0.36
Les Miserables (1)	77	6.6	2.6	-0.16	0.74	0.47	0.53	0.25	0.16
Genes									
Human Gene 1 (1)	22282	15	5.3	0.068	0.66	0.52	0.69	0.59	0.53
Human Gene 2 (1)	14337	19	3.6	-0.0047	0.65	0.46	0.6	0.56	0.55
Mouse Gene (1)	45101	5.5	4.9	0.3	0.57	0.51	0.74	0.6	0.59
Language									
Reuters News 9/11 (1)	13314	22	3.1	-0.11	0.39	0.22	0.24	0.2	0.14
Language Free Assoc. (1)	10617	6.8	4.8	-0.0076	0.13	0.12	0.52	0.37	0.23
Collaboration									
Condensed Matter (1)	16726	5.7	6.6	0.18	0.74	0.74	0.52	-0.16	-0.19
High Energy Physics (1)	8361	3.8	7	0.29	0.64	0.63	0.52	-0.091	-0.13
Astrophysics (1)	16706	15	4.8	0.24	0.73	0.72	0.53	-0.04	-0.19
Network Science (1)	1589	3.5	5.8	0.46	0.88	0.87	0.61	-0.042	-0.43
Learning									
LSCrit (10)	60	11	2.3 ± 0.03	0.12 ± 0.04	0.68	0.44	0.78 ± 0.06	0.15	0.27
LSSub (10)	60	11	2.3 ± 0.04	0.15 ± 0.02	0.67	0.43	0.79 ± 0.02	0.17	0.016
LSSup (10)	60	11	2.3 ± 0.02	0.15 ± 0.03	0.68	0.44	0.64 ± 0.14	0.075	0.25
ASCrit (10)	60	11	2.3 ± 0.05	0.15 ± 0.03	0.68	0.44	0.44 ± 0.04	-0.1	-0.059
ASSub (10)	60	11	2.3 ± 0.03	0.15 ± 0.03	0.68	0.44	0.33 ± 0.02	-0.11	-0.21
ASSup(10)	60	11	2.3 ± 0.04	0.15 ± 0.04	0.68	0.44	0.47 ± 0.01	-0.0011	6.3e-16
Models									
OHO Type I (10)	100	12	2.7 ± 0.06	0.2 ± 0.015	0.67	0.52	0.57 ± 0.01	-0.0023	-0.011
OHO Type II (10)	100	12	2.7 ± 0.07	0.2 ± 0.016	0.67	0.52	0.5 ± 0.01	-0.41	-0.41
OHO Type III (10)	100	12	2.7 ± 0.07	0.19 ± 0.03	0.67	0.52	0.65 ± 0.01	0.58	0.55
WN Type I (10)	100	9.8	2.5	-0.03 ± 0.03	0.46	0.37	0.56 ± 0.01	0.0063	-0.005
WN Type II (10)	100	9.8	2.5	-0.01 ± 0.04	0.46	0.37	0.54± 0.01	-0.4	-0.13
WN Type III (10)	100	9.8	2.5 ± 0.05	0.05 ± 0.04	0.46	0.4	0.6 ± 0.01	0.4	0.48
Growth Models									
GM1 OHO W_1 (10)	100	12	2.7 ± 0.03	0.19 ± 0.02	0.67	0.52	0.5 ± 0.01	-0.46	-0.3
GM2 OHO W_2 (10)	60	11	2.3 ± 0.04	0.2 ± 0.03	0.67	0.43	0.5 ± 0.01	0.038	-0.17

5. Supplementary Figures

Figure S1 | Integrative weight organization for gene networks is also obtained when reducing network size by random node sub-sampling instead of removal of weakest links, e.g. 0.08 threshold used in figure 1. a, Results obtained by sub-sampling N = 2,000 nodes from the original gene networks. For each genome, five sub-sampled networks were averaged and their link clustering analysis (left) and pruning analysis (right) are shown. **b**, Corresponding analysis for sub-sampling N = 1,000 nodes (10 subsamples averaged for each genome).

Figure S2 | **Visualization of the trend in link clustering. a**, Plot of C_L vs. link weight rank for every link in eight different networks as labelled. Note that these plots reveal that the values of C_L are very heterogeneous at every weighting level, but also show trends consistent with those visualized using average values within ten bins (*cf*. Fig. 1 main text). **b**, Distributions of C_L values are plotted for each bin for different networks. For the integrative networks the distributions, while being very broad, are reasonably well localized and show clear increasing trend.

Figure S3. | **Definition of excess node clustering. a**, Bottom–pruning analysis of the node clustering coefficient C for n = 7 weighted, directed functional neuronal avalanche networks. ΔC: excess node clustering. *DSPR*: degree–sequence preserved randomization. **b**, Single example of a bottom–pruned network at f = 0.3 and 0.9 indicated by red arrows in left panel.

Figure S4 | Changes in ΔC are the result of changes in C_{orig}, and C_{DSPR}, so the same change in excess clustering can be obtained in many different ways. To obtain a more detailed picture, the same networks and weight organizations as in Figure 3 in the main text are shown here with both C_{orig} (solid lines) and C_{DSPR} (broken lines) plotted separately, with left panels showing bottom–pruning and right top–pruning. **a**, Bottom – pruning (left) and top–pruning (right) of OHO (black) and WN (blue) neutral networks (solid lines) and corresponding DSPR controls (broken lines; n = 10). Note linear decay as predicted by theory for both the original and randomized controls. **b**, For bottom–pruning, C remains relatively high in this dispersive network model, but the increase in C_{DSPR} leads to an overall reduction in ΔC, particularly for OHO topology. **c**, Conversely, C_{DSPR} increases for top– but not bottom–pruning in integrative networks. The symmetry between the integrative vs. dispersive and bottom vs. top pruning for OHO topology is the result of its inverse linear relationship between the node clustering coefficients and degrees. In most topologies, node clustering coefficient and node degree are inversely related, $C \sim k^{-\beta}$, with $0<\beta<1$ and thus we expect similar results in other topologies.

Figure S5 | Same simulations as in figure 3 main text, but now using the "all" definition for the neighbourhood in directed networks, showing virtually the same results. **a**, Neutral networks with independent link weights implemented on OHO (black) and WN (red) topologies. *Left*: ΔC_L does not correlate with weight rank. *Right*: ΔC decreases monotonically with f for bottom– (*solid lines*) and top–pruning (broken lines). **b**, Corresponding analysis for dispersive networks where w_{ij} are assigned as the

geometric mean of the end-node degrees k_i and k_j . **c**, Corresponding analysis for integrative networks. See main text Figure 3 for further details. Simulations of n = 10 networks each (N = 100; <k> = 12, 10 for OHO, WN).

Figure S6 | Scatter plot of M and R_{C_L} for directed weighted networks (see Suppl. Table and Fig. 4 main text for details) using different definitions of neighbourhood. *Src*: Source node; *Targ*: Target node. We see that R_{C_L} is very robust to the choice of neighbourhood, while M shows greater variability. Nevertheless, classification of networks into dispersive, neutral, and integrative is fairly robust to neighbourhood definition. For network legend see Fig. 4 main text and Fig. S9.

Figure S7 | Link clustering trends and robustness to pruning for evolving network models (**a**) GM1 applied to OHO growth model. (**b**) GM2 applied to OHO growth model.

Figure S8 | We explored the relationship between the two measures of weight organization, *M* and R_{C_L} . **a**, Recurrence plot of M vs. R_{C_L} during last step learning. Plot covers learning from the 100,000 to 10 million learning steps (same values as in Fig. 6c, d). Average of n = 10 networks. While both M and R_{C_L} remain in the positive quadrant, their trends during learning are fairly un-correlated (R = -0.24) which suggests that a simple monotonically increasing relationship between measures M and R_{CL} does not exist. **b,** Implementation of the weighted social network model[13] for two different values of p_Δ , p_Δ =0.001 and p_Δ =0.005, as indicated, and three values. All models were

run between 10 and 25 node generations, i.e. that many times each node was on average removed randomly, together with all of its links. In most cases it took less than 5 generations for the main network parameters to became stationary (e.g. average degree and clustering coefficient). We report the values of R_{C_L} and *M* during the stationary period. The results indicate that R_{C_L} does provide constraints for *M* however their values are uncorrelated during the time evolution. Furthermore (see also Fig. 4), its *M* is lower than the one observed in real world networks. **c,** Results for OHO and WN topologies using 16 different values for parameter *a* in Eq. S5, approximately logarithmically spaced between 0.01 and 100. Three different network sizes were used N = 60 (black), N = 100 (blue), N = 200 (red). These results indicate that of R_{C_L} does not always constrain the values of M to be in the positive/negative quadrant, nor the passage through the origin of their trajectory. From these results and other results we can only say that having positive R_{C_L} is necessary but not sufficient condition for having high robustness observed in some biological networks.

Figure S9 | Comparison of R_{C_L} with alternative network measures. a, R_{C_L} correlates with R_w as described in Eq. S4. Thus, link weights organize along two different local measures of clustering, the relative fraction of common neighbours, and the clustering coefficients of the corresponding end nodes. **b**, The local measure R_{C_L} positively correlates with modularity Q, a global measure of community structure, which in the current analysis takes link weight into account (R = 0.35) [26].

Reference List

1. Watts,D.J. & Strogatz,S.H. Collective dynamics of 'small-world' networks. *Nature* **393**, 440-442 (1998).

2. Radicchi,F., Castellano,C., Cecconi,F., Loreto,V., & Parisi,D. Defining and identifying communities in networks. *Proc. Natl. Acad. Sci. U. S. A* **101**, 2658-2663 (2004).

3. Maslov,S. & Sneppen,K. Specificity and stability in topology of protein networks. *Science* **296**, 910-913 (2002).

4. Newman,M.E.J. Properties of highly clustered networks. *2003* **68**, 026121 (2003).

5. Ravasz,E. & Barabasi,A.L. Hierarchical organization in complex networks. *Phys Rev. E. Stat. Nonlin. Soft. Matter Phys* **67**, 026112 (2003).

6. Dorogovtsev,S.N. & Mendes,J.F.F. *Evolution of networks: From biological nets to the internet and WWW*(University Press, Oxford, USA, 2003).

7. Dorogovtsev,S.N. & Mendes,J.F.F. Evolution of networks. *Advances in Physics*1079-1187 (2002).

8. Boguna,M., Krioukov,D., & Claffy,K.C. Navigability of complex networks. *Nature Physics* **5**, 74-80 (2008).

9. Serrano,M.A., Krioukov,D., & Boguna,M. Self-similarity of complex networks and hidden metric spaces. *Phys Rev. Lett.* **100**, 078701 (2008).

10. Newman,M.E. & Watts,D.J. Scaling and percolation in the small-world network model. *Phys Rev. E. Stat. Phys Plasmas. Fluids Relat Interdiscip. Topics.* **60**, 7332-7342 (1999).

11. Ozik,J., Hunt,B.R., & Ott,E. Growing networks with geographical attachment preference: emergence of small worlds. *Phys Rev. E. Stat. Nonlin. Soft. Matter Phys* **69**, 026108 (2004).

12. Barabasi,A.L. & Albert,R. Emergence of scaling in random networks. *Science* **286**, 509-512 (1999).

13. Kumpula,J.M., Onnela,J.P., Saramaki,J., Kaski,K., & Kertesz,J. Emergence of communities in weighted networks. *Phys Rev. Lett.* **99**, 228701 (2007).

14. Pajevic,S. & Plenz,D. Efficient network reconstruction from dynamical cascades identifies small-world topology from neuronal avalanches. *PLoS Comp. Biol.* **5**, e1000271 (2008).

15. Beggs,J.M. & Plenz,D. Neuronal avalanches in neocortical circuits. *J. Neurosci.* **23**, 11167-11177 (2003).

16. Plenz,D. & Chialvo,D.R. Scaling properties of neuronal avalanches are consistent with critical dynamics. *arXiv:0912. 5369*(2010).

17. Petermann,T. *et al.* Spontaneous cortical activity in awake monkeys composed of neuronal avalanches. *Proc. Natl. Acad. Sci. U. S. A* **106**, 15921-15926 (2009).

18. Hagmann,P. *et al.* Mapping the structural core of human cerebral cortex. *PLoS. Biol.* **6**, e159 (2008).

19. Gregoretti,F., Belcastro,V., di Bernardo,D., & Oliva,G. A parallel implementation of the network identification by multiple regression (NIR) algorithm to reverse-engineer regulatory gene networks. *PLoS ONE.* **5**, e10179 (2010).

20. Gardner,T.S., di Bernardo,D., Lorenz,D., & Collins,J.J. Inferring genetic networks and identifying compound mode of action via expression profiling. *Science* **301**, 102-105 (2003).

21. Knuth,D.E. *The Stanford GraphBase: A Platform for Combinatorical Computing*(Addison-Wesley, Reading, MA, 1993).

22. Varshney,L.R., Chen,B.L., Paniagua,E., Hall,D.H., & Chklovskii,D.B. Structural properties of the *Caenorhabditis elegans* neuronal network. *arXiv:0907. 2373v2*(2010).

23. White,J.G., Southgate,E., Thomson,J.N., & Brenner,S. The structure of the nervous system of the nematode Caenorhabditis elegans. *Phil. Trans. R. Soc. Lond.* **314**, 1-340 (1986).

24. Yook,S.H., Jeong,H., Barabasi,A.L., & Tu,Y. Weighted evolving networks. *Phys. Rev. Lett.* **86**, 5835-5838 (2001).

25. Barrat,A., Barthelemy,M., & Vespignani,A. Weighted evolving networks: coupling topology and weight dynamics. *Phys Rev. Lett* **92**, 228701 (2004).

26. Girvan,M. & Newman,M.E. Community structure in social and biological networks. *Proc. Natl. Acad. Sci. U. S. A* **99**, 7821-7826 (2002).

27. Newman,M.E.J. Analysis of weighted networks. *Phys. Rev. E.* **70**, 056131 (2004).

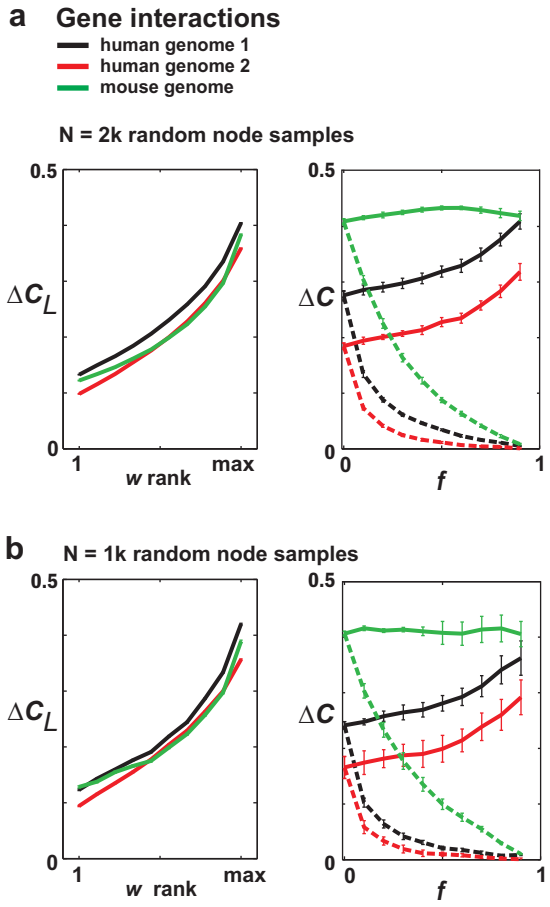

Pajevic &Plenz
Figure S1
Gene Subsample
1 col

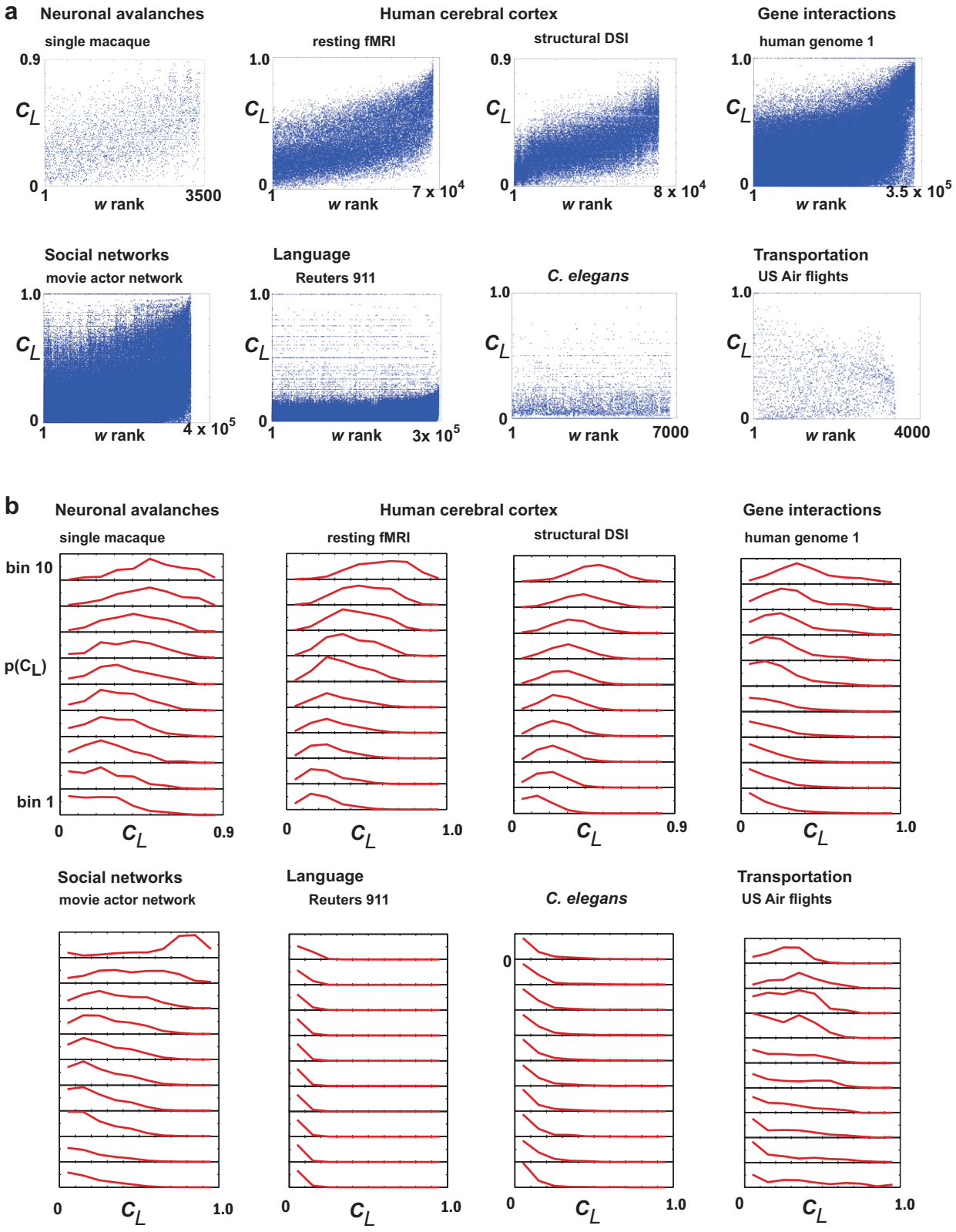

Pajevic &Plenz
Figure S2
dC_L distributions

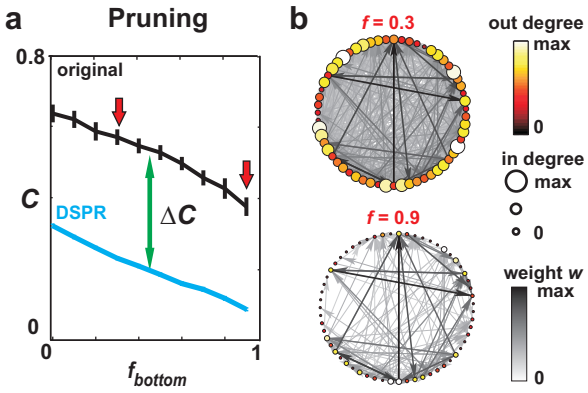

Pajevic &Plenz
Figure S3
Methods
2 cols

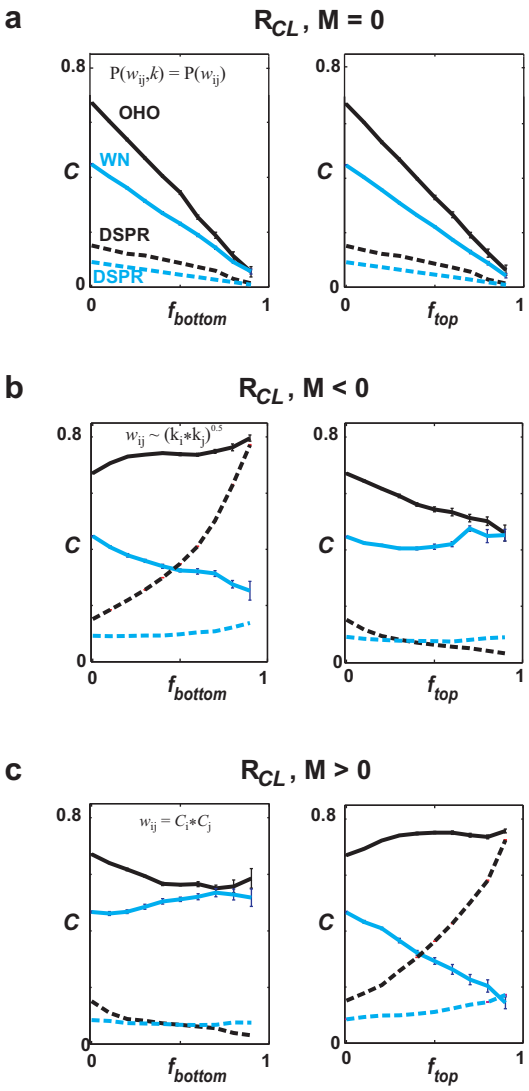

Pajevic &Plenz
Figure S4
Model C
2 col

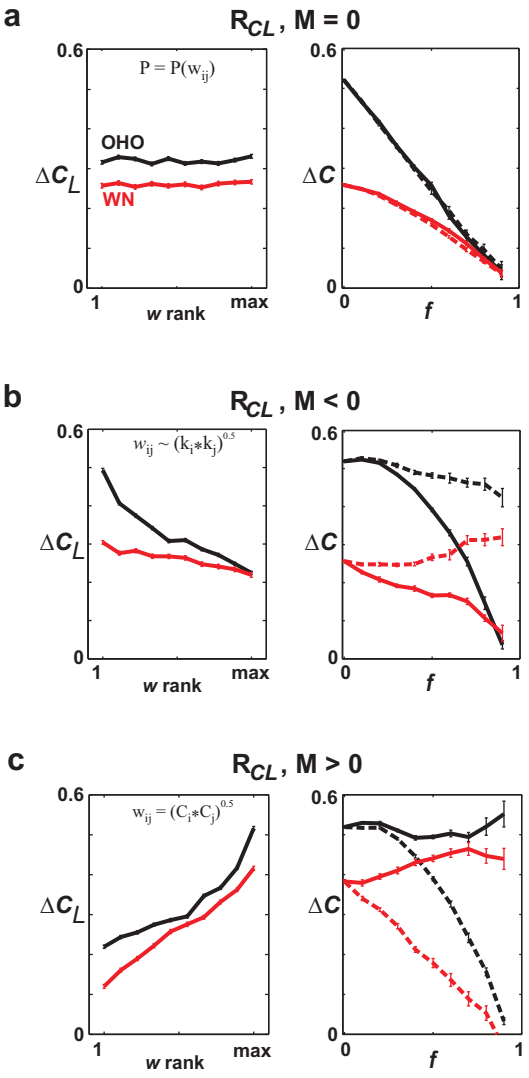

Pajevic &Plenz
Figure S5
All NN
2 col

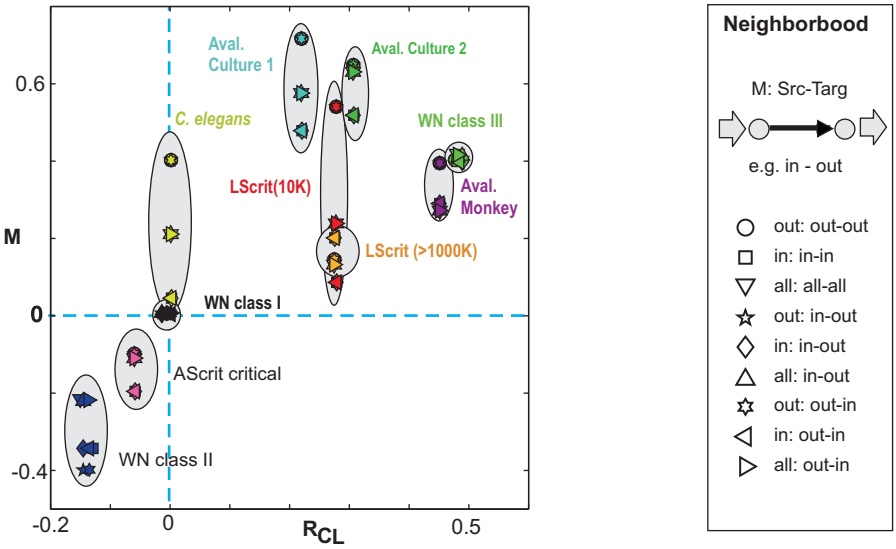

Pajevic &Plenz
Figure S6
NN dependency
1.5 col

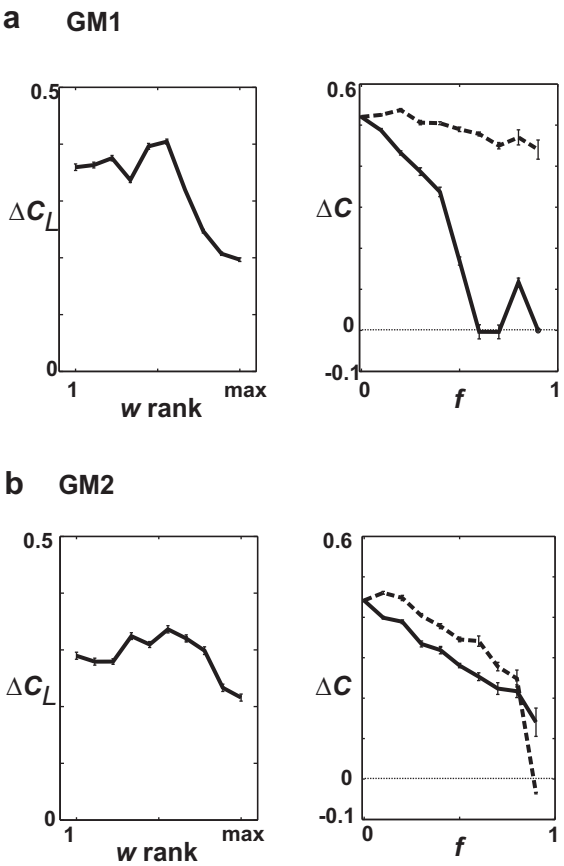

Pajevic &Plenz
Figure S7
Growth models
1 col

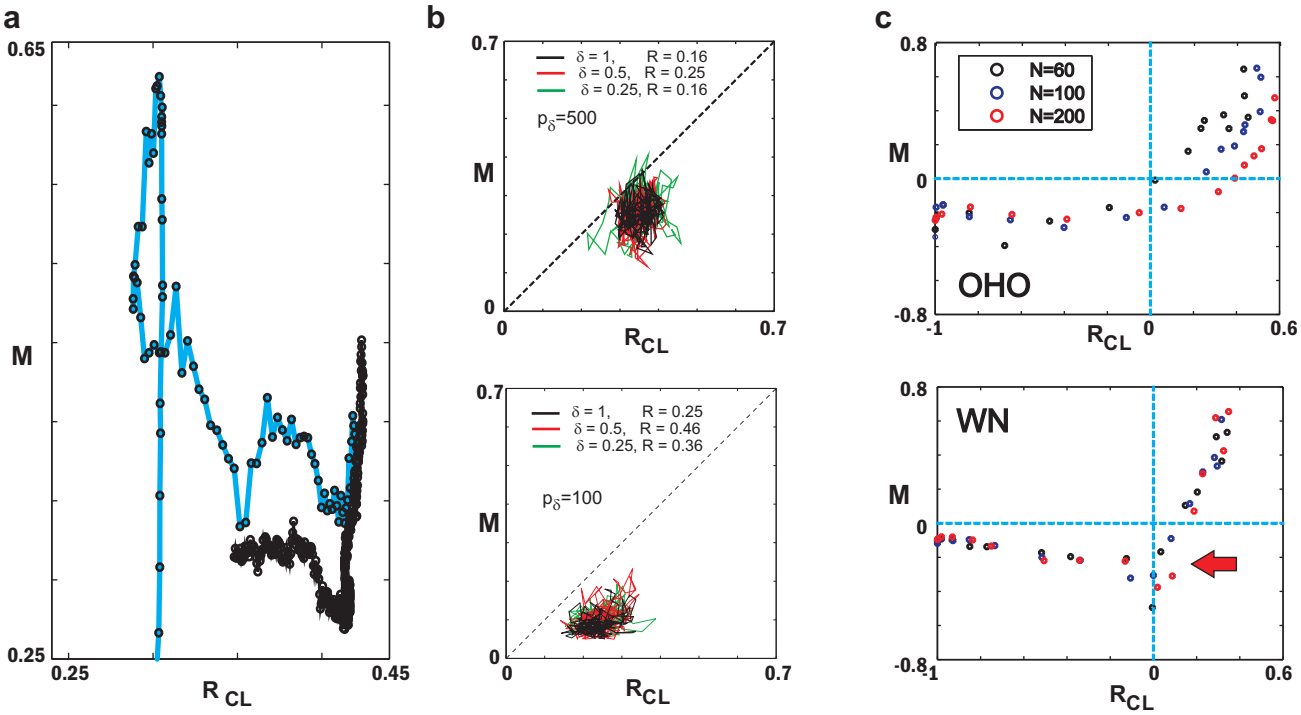

Pajevic &Plenz
Figure S8
Decorr Rcl & M
1 col

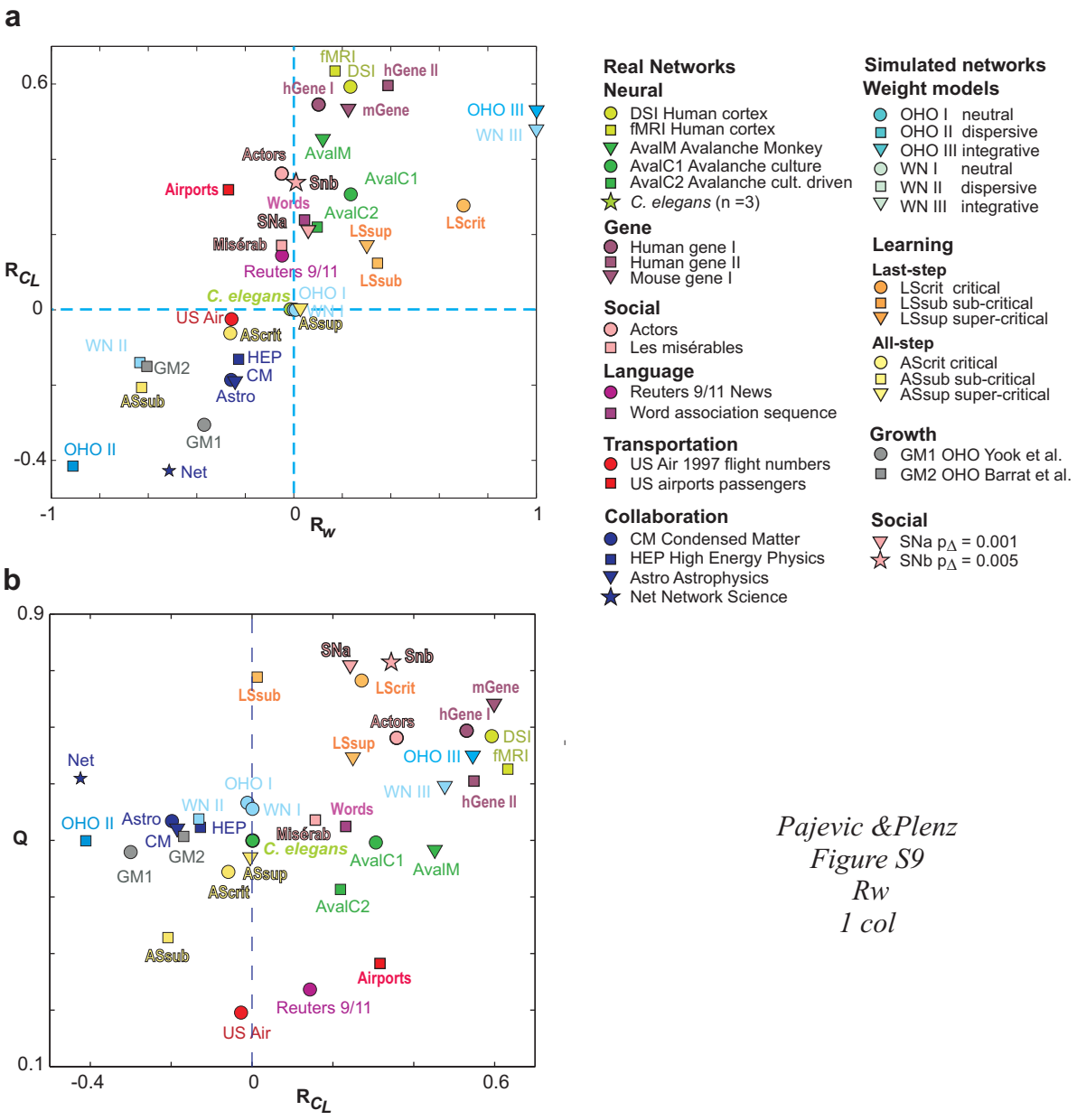

Pajevic &Plenz
Figure S9
Rw
1 col